Influence of Nanoparticle Coating on the Differential Magnetometry and Wireless Actuation of Biohybrid Microrobots

Magdanz, Veronika; Cumming, Jack R. ; Salamzadeh, Sadaf ; Tesselaar, Sven ; Alic, Lejla ; Abelmann, Leon; Khalil, Islam S.M.

DOI
10.1109/IROS55552.2023.10341258

Publication date
2023

Document Version
Final published version

Published in
Proceedings of the 2023 IEEE/RSJ International Conference on Intelligent Robots and Systems (IROS)

2023 IEEE/RSJ International Conference on Intelligent Robots and Systems (IROS)
October 1-5, 2023. Detroit, USA

Influence of Nanoparticle Coating on the Differential Magnetometry and Wireless Actuation of Biohybrid Microrobots

Veronika Magdanz*, Jack R. Cumming†, Sadaf Salamzadeh‡,
Sven Tesselaar‡, Lejla Alic‡, Leon Abelmann⋆, and Islam S. M. Khalil†

2023 IEEE/RSJ International Conference on Intelligent Robots and Systems (IROS) | 978-1-6654-9190-7/23/$31.00 ©2023 IEEE | DOI: 10.1109/IROS55552.2023.10341258

***Abstract*— Magnetic nanoparticles can be electrostatically assembled around sperm cells to form biohybrid microrobots. These biohybrid microrobots possess sufficient magnetic material to potentially allow for pulse-echo localization and wireless actuation. Alternatively, magnetic excitation of these nanoparticles can be used for localization based on Faraday's law of induction using a detection coil. Here, we investigate the influence of the electrostatic attraction between positively charged nanoparticles and negatively charged sperm cells on the activation of the nanoparticles during nonlinear differential magnetometry and wireless magnetic actuation. Activation of clusters of free nanoparticles and nanoparticles bound to the body of sperm cells is achieved by a combination of a high-frequency alternating field and a pulsating static field. The nonlinear response in both cases indicates that constraining the nanoparticles is likely to yield significant decreases in the magnetometry sensitivity. While the attachment of particles to the cells enables wireless actuation (rolling locomotion), the rate of change of the magnetization of the nanoparticles decreases one order of magnitude compared to free nanoparticles.**

I. INTRODUCTION

There is a significant interest in the use of biohybrid microrobots in biomedical applications such as drug and cell delivery [1]. The key advantage of these biohybrid microrobots, which consist of biological cells and artificial components, over solely synthetic microrobots is their biocompatibility, flexibility, facile loading with a cargo, and adaptability [2]. There is excessive research involving microorganisms or cells for propulsive thrust or locomotion [3], [4]. In case of biohybrid microrobots consisting of a living organism, there are strict limitations that biological considerations will impose on any environment and design. It may be challenging to provide the favorable biological condition necessary for biohybrid microrobots to function.Alternatively, biohybrid microrobots which use organisms/cells regardless of their viability ourely as structural biotemplates does not impose limitations on the surroundings or the operation time and therefore enables motion control regardless without time or environmental constraints(e.g., pH, temperature, nutritional levels) [5]-[10]. Magnetically actuated biohybrid microrobots, as also presented in this article, use magnetic nanoparticles (MNPs) attached to the surface of the cells (Figs. 1(A) and 1(B)) [11]-[13]. In contrast to the cell-driven biohybrid microrobots, which have potential assisted fertilization, these sperm cell-templated microrobots have potential for drug delivery and imaging in the reproductive tract, for which the viability is irrelevant.

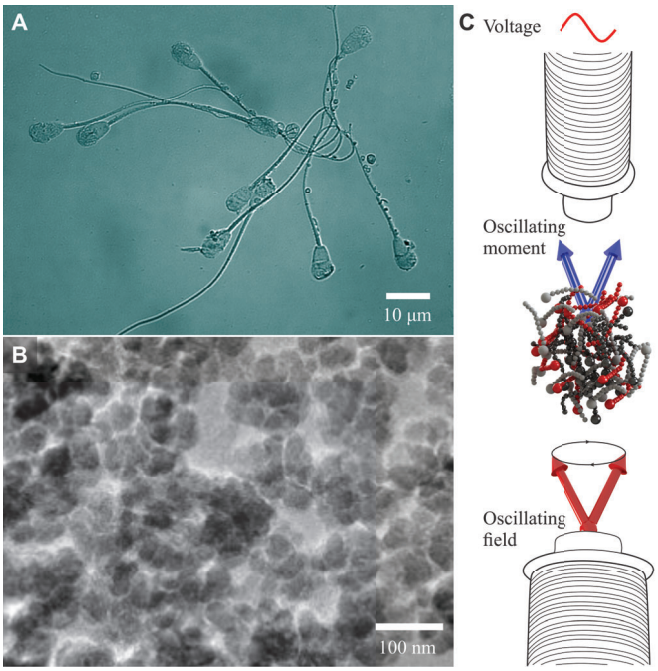

Fig. 1. The magnetic nanoparticles (MNPs) attachment to the organic body of sperm cells incorporate additional functionality, allowing for actuation and noninvasive localization. (A) MNPs-coated dead bovine sperm cells. Mechanical entanglement between MNPs-coated cells provides clusters, offering advantages for drug loading, localization and actuation. (B) Transmission electron microscopy micro-graphs (FEI Tital Themis Cubed) of the MNPs used to magnetize the cells: Synomag®D-70 with the core diameter of 29 ± 4 nm. The images are acquired using an accelerating voltage of 300 kV and a pixel size of 0.15 nm. (C) A voltage signal can be picked up using a detection coil, upon applying an oscillating field using excitation coils.

Magnetic nanoparticles (MNPs) have proven to be successful as biocomatible yet potent material to generate magnetic signal in the human body. MNPs have been deposited onto organic components by sequential deposition allowing the resulting biohybrid microrobots to move in response to applied fields. Yan *et al*. have demonstrated a dip-coating approach of *Spirulina* microalgae with magnetite nanoparticles, creating microrobots with intrinsic fluorescence, desirable cytocompatibility, and natural degradability [12]. Sperm cells

*V. Magdanz is with the Department of System Design Engineering, University of Waterloo, ON N2L 3G1 Waterloo, Canada.
†The authors are with the Department of Biomechanical Engineering, University of Twente, 7500 AE Enschede, The Netherlands.
‡The authors are with the Magnetic Detection & Imaging group, Technical Medical Centre, University of Twente, 7500 AE Enschede, The Netherlands.
⋆L. Abelmann is with the Department of Microelectronics, Delft University of Technology, 2600 AA Delft, The Netherlands.
This work was supported by the Twente University RadBoudumc Opportunities (TURBO) program 2022 and Grant Crazy-Research-2022.

offer a great template for flexible microswimmers due to their flagellum that can perform undulatory motion under influence of a rotating field. Middelhoek *et al*. have fabricated clusters of MNPs-coated sperm cells as biohybrid microrobots exibiting predicable rolling locomotion under a rotating field, and improved ultrasound detectability [14]. In addition to locomotion, the MNPs also produce a measurable radio-frequency (RF) signal resulting from the actuation by external field. This signal can potentially be utilized for localization of MNPs-coated clusters. However, the dynamic behaviour of MNPs in a time-varying magnetic field is complex, especially in the domain where simultaneous Brownian and Néel processes take place. Brownian relaxation aligns the whole particle with the field, while Néel relaxation aligns the internal magnetic dipole within the particle. Previous research also revealed that magnetic response of MNPs to actuation signal decreases with increased medium viscosity or the size of the MNPs [6]. As quality of magnetic sensing depends on the targeted actuation and accurate acquisition of MNPs response, the locomotion needs to be optimized for the size of microrobots and MNPs properties. In addition, the magnetic response of rigidly attached MNPs to the cell membrane should be understood. We aim to achieve simultaneous localization and actuation using differential magnetometry and the permanent magnet-based robotic system, respectively.

Differential magnetometry differs from the pulse-echo techniques [15] in that the response of nanoparticles and the surrounding tissue to excitation are highly different, allowing highly specific MNPs localization even when completely surrounded by tissue [16]. This detection method potentially allows optimization by changing actuation parameters. This paper provides an experimental work aiming to assess the potential of a complete magnetic control and simultaneous localization of biohybrid microrobots. Therefore, we address all individual components separately, starting with the response of MNPs to a specific actuation and the changes in the response due to coating onto the sperm cells, using differential magnetometry measurements and nanoparticles that are electrostatically assembled around sperm cells [17]. Their oscillating magnetization is measured in terms of the induction voltage in a detection coil configuration. We focus on the effect of the electrostatic-based self-assembly between the organic body of sperm cells and the MNPs on the sensitivity of the differential magnetometry that is measured by a laparoscopic differential magnetometer and a super paramagnetic quantifier (Fig. 1(C)). We begin by conducting an experimental comparative study between a colloidal solution of unbound MNPs and constrained MNPs that are electrostatically attached to the organic body of the sperm cells. An alternating field magnetometer and a permanent-magnet robotic system are used to measure the response of the nanoparticles in these two cases (Fig. 2).

The remainder of this paper is organized as follows: Section II includes the basic principles of magnetic actuation and differential magnetometry for clusters of MNPs coated-sperm cells. Characterization results of gravity-assisted locomotion

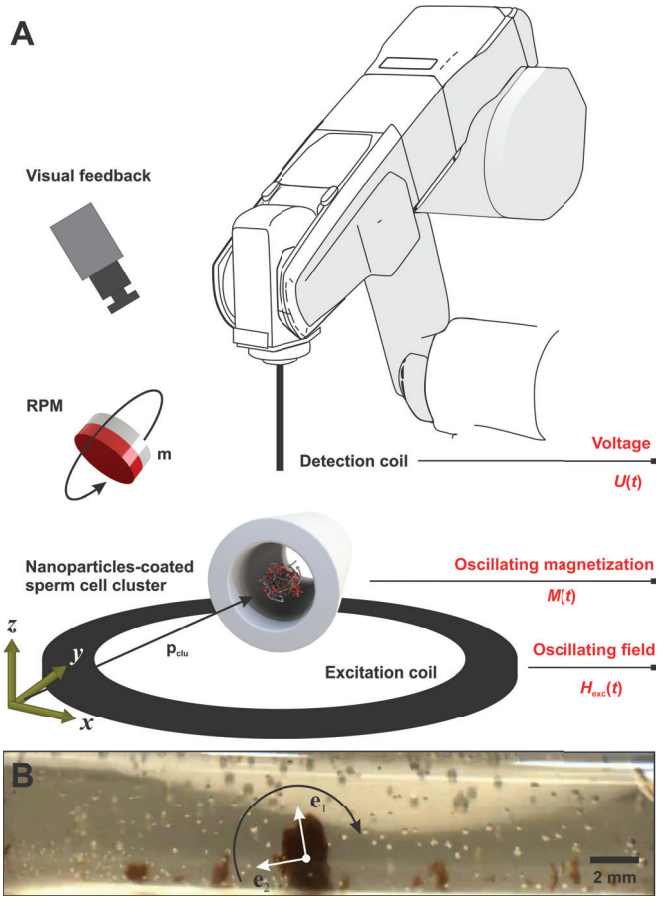

Fig. 2. Illustration of the main components necessary for a complete magnetic locomotion (i.e., actuation and control). (A) Actuation of MNPs-coated cells is accomplished by a rotating permanent magnet (RPM) while control-input is enabled by magnetic sensing and warranted by an oscillating magnetic field $\mathbf{H}_{\mathrm{exc}}$ produced by an excitation coil. The excitation coil provides an oscillating magnetic field, $\mathbf{H}_{\mathrm{exc}}$, and the resulting oscillating magnetization, $M(t)$, of the cluster is picked up by the detection coil as voltage, $U(t)$. (B) A cluster of MNPs-coated sperm cells rolls inside a lumen using a rotating magnetic field. The unit vectors $\mathbf{e}_1$ and $\mathbf{e}_2$ define the directions of the demagnetizing factors, n_{a} and n_{r}, of Equation 4.

and response of the clusters using laparoscopic differential magnetometry and super paramagnetic quantifier are presented in Section III. Discussions pertaining to the potential solutions and fabrication methods for the detection of the magnetic response of the biohybrid clusters are provided in Section IV. Finally, Section V concludes and provides direction for future work.

II. Actuation and Localization of Magnetic Nanoparticles-Coated Sperm Cells

Submillimeter-sized clusters of MNPs-coated sperm cells are magnetized to a magnetic moment when external field is applied, allowing for directional control and inductive response that can be detected using a nearby detection coil, as shown in Fig. 2. If the external magnetic field includes components with different frequencies, then the low-frequency component will allow directional control and locomotion, whereas the high-frequency component (in the kilohertz range) will result in an oscillating magnetization

and its response can be detected based on Faraday's law of electromagnetic induction in terms of a voltage, $U(t)$. These two components are generated using an excitation coil generating excitation field, $\mathbf{H}_{\rm exc}$, and a rotating permanent magnet (RPM) of magnetic moment $\mathbf{m}$.

A. Localization using High-Frequency Magnetic Excitation

We consider MNPs, either free or attached to an organic body, of magnetization $\boldsymbol{M}$. The location of the cluster is characterized by the position vector $\mathbf{p}_{\rm clu}$ with respect to a frame of reference (Fig. 2). The cluster is contained inside a transparent fluid-filled lumen (internal diameter of a few millimeters) that is fixed with respect to an excitation coil in the $\boldsymbol{x}$-$\boldsymbol{y}$ plane. The RPM and the detection coil are robotically moved and their motion is characterized by the position vectors ${}^0\mathbf{p}_{\rm rpm}$ and ${}^0\mathbf{p}_{\rm det}$ with respect the reference frame, respectively. When the excitation coil is provided with current, $I_{\rm exc}$, we obtain magnetic field as [18]

$$H_{\rm exc} = S_{\rm exc}\frac{I_{\rm exc}\sin\omega t}{\mu_0}, \tag{1}$$

where $S_{\rm exc}$ is the excitation coil's constant, ω is the oscillation frequency, and μ_0 is the permeability of free space. For an oscillating field, $H_{\rm exc}$, generated by the excitation coil, the ratio between the magnetic and thermal energy, χ, is given by

$$\chi = \frac{\mu_0 m H_{\rm exc}}{k_{\rm B}T}, \tag{2}$$

where $k_{\rm B}$ and T are the Boltzmann constant and the absolute temperature, respectively. If the oscillating field is applied on MNPs of saturation magnetization $M_{\rm s}$, then the oscillating magnetization of the particles can be approximated as

$$M = M_{\rm s}\mathcal{L}(\chi), \tag{3}$$

where $\mathcal{L}(\chi) = \coth\chi - 1/\chi$. The oscillating magnetization is often observed through an inductive response within a nearby detection coil (Fig. 2), in which the induced voltage scales with the amount of nanoparticles and the localization gap (distance between the detection probe and the cluster).

B. Rotation using Low-Frequency Actuation

In contrast to high-frequency magnetic excitation, locomotion requires rotation of the external field at low-frequencies, below a step-out frequency, $\omega_{\rm so}$, that is given by

$$\omega_{\rm so} = \frac{\mu_0|\mathbf{H}_{\rm act}||n_{\rm a}-n_{\rm r}|V}{2n_{\rm a}n_{\rm r}f_{\rm r}}, \tag{4}$$

where $\mathbf{H}_{\rm act}$ is the actuation field and $f_{\rm r}$ is the rotational drag coefficient of the cluster. Further, V is the volume of the cluster, $n_{\rm a}$, and $n_{\rm r}$ are the demagnetizing factor in the preferred magnetization direction of the cluster (i.e., $\mathbf{e}_1$ in the coordinate system in Fig. 2(B)) and the demagnetizing factor in the direction perpendicular to the preferred magnetization direction (i.e., $\mathbf{e}_2$), respectively. Rolling of the cluster with respect to the detection coil would allow a greater signal to be measured as the localization gap decreases. The induction voltage in the detection coil is proportional to the time-derivative of the magnetization (i.e., $U(t) \propto {\rm d}M/{\rm d}t$) and scales with the localization gap. Therefore, it is possible to actuate and excite the cluster using $\mathbf{H}_{\rm act}$ and $\mathbf{H}_{\rm exc}$ with the wireless manipulation and magnetometer systems (Fig. 2). The average angular velocity of the cluster is approximated by

$$\omega_{\rm c} = \omega_{\rm f}\left(1-\sqrt{1-\left(\frac{\omega_{\rm so}}{\omega_{\rm f}}\right)^2}\right), \tag{5}$$

where $\omega_{\rm c}$ is the average angular velocity of the cluster and $\omega_{\rm f}$ is the frequency of the field. For a given actuation frequency, $\omega_{\rm f}$, Equations (4) and (5) can be used to calculate the rolling velocity assuming no slipping.

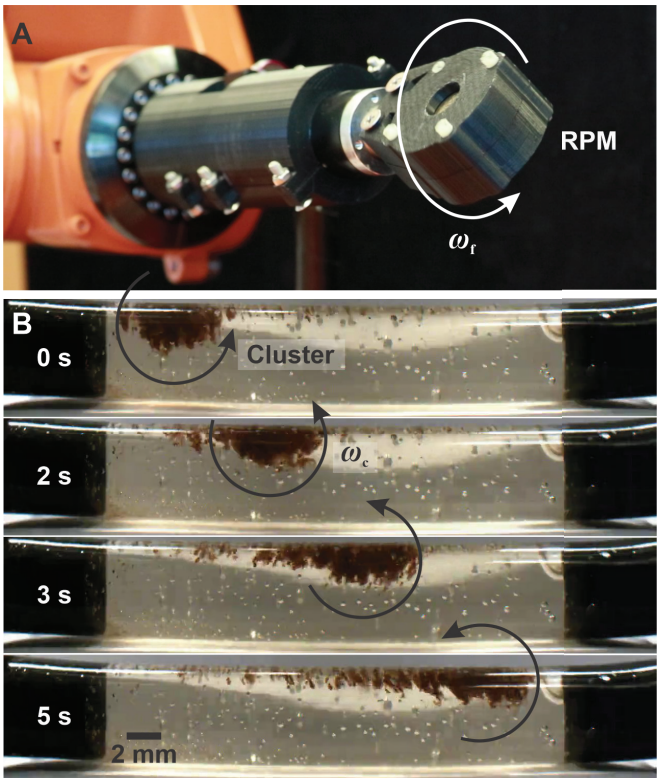

Fig. 3. Wireless actuation of the clusters is achieved using a low-frequency rotating field, generated using a rotating permanent magnet (RPM). (A) The position of the RPM is controlled robotically using a manipulator. The rotation-axis of the RPM is fixed at $[1,0,0]^T$ with respect to the frame of reference in Fig. 2. (B) The cluster rolls under the influence of the rotating field and a pulling force. The actuation frequency of the RPM is 1.6 Hz and the field is 9.3 mT. The field-gradient pulling is adjusted using the RPM-cluster-gap. Please see supplementary multimedia.

III. Experimental Results

The biohybrid clusters (containing MNPs-coated sperm cells) are investigated regarding their actuation in a low frequency (0.01-10 Hz) rotating field generated by a rotating permanent magnet. The dynamic magnetic properties of the nanoparticles and biohybrid clusters are assessed using a superparamagnetic quantifier (SPaQ) [8]. The signal produced by the actuated clusters is assessed using prototype devices utilising differential magnetometry [9].

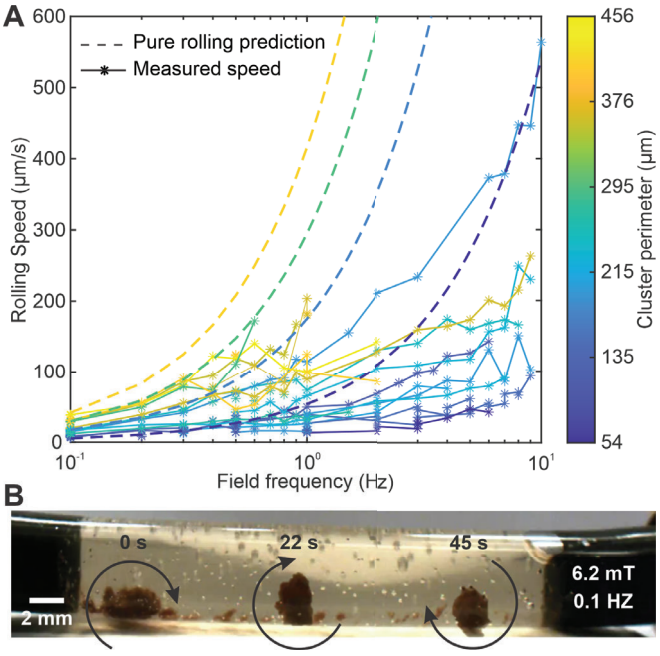

Fig. 4. The rolling velocity of clusters of magnetic nanoparticles-coated sperm cells is calculated and measured for actuation frequency range of 0.1:10 Hz for clusters with perimeter in the $54\,\mu m$ to $456\,\mu m$ range. The rolling speed is calculated based on Equation (5). (A) The rolling velocity of the cluster increases with the actuation frequency and the perimeter. (B) A representative wireless actuation of a cluster shows rolling locomotion at 0.1 Hz and magnetic field of 6.2 mT. Please see supplementary multimedia.

A. Fabrication of the Biohybrid Clusters

Similarly to a previously reported method [11], the biohybrid clusters are produced by electrostatic-based self-assembly using negatively charged sperm cells and positively charged MNPs. Dextran coated flower shaped MNPs, Synomag®D-70 (Micromod Partikeltechnologie GmbH) with hydrodynamic diameter of 70 nm are utilized. Cryopreserved bovine semen is thawed in a 37°C water bath for 2 min, before diluting the semen in 1 mL Phosphate buffer saline (Thermo Scientific Gibco). The sperm cell sample containing 10^7 cells/mL was centrifuged at 300 g for 5 min, the supernatant removed and resuspended in distilled water. This washing step is repeated twice before adding 100 µL of the 70 nm Synomag®D-70 nanoparticles to 900 µL of cell suspension, resulting in a final concentration of 2.5 mg/mL of particles. These particle-covered sperm cells form clusters of different sizes due to the entanglement of the sperm cells, which increases the overall magnetic material per tracked object. Each cluster is approximated by an ellipsoid with demagnetizing factors n_a and n_r in the direction of the orthonormal vectors $\mathbf{e}_1$ and $\mathbf{e}_2$, respectively (Fig. 2(B)).

B. Wireless Actuation

A whole setup (illustrated in Fig. 2) addressing biohybrid microrobots consists of a magnetic actuation, visual feedback, and magnetic sensing for localization purposes. An RPM is robotically actuated to control the magnetic moment rotation axis and the field rotation axis at the position of the cluster. The rotating field allows for a controllable movement of cell clusters inside a fluid-filled tube, as shown in Fig. 2(B). The magnetic moment of the RPM is orthogonal to its rotation axis (Fig. 3(A)), and to the long axis of the lumen, allowing the cluster to move along the $\pm\boldsymbol{y}$-axis of the tube (illustrated in Fig. 2). Small distances between the RPM and the lumen allow the magnetic force to pull the MNPs-cluster in a rolling motion. Depending on amplitude of the pulling force, the MNPs-clusters roll along the upper side of the lumen (larger forces) or along the lower side of the lumen (smaller forces), as shown in Fig. 3(B). The rolling speed of the clusters depends on their size, so that the cluster spreads out over the tube. When the rotational frequency of the field becomes too high, the clusters start breaking up (see Fig. 3(B)).Rotational speed should be kept in the low frequency range to avoid this effect. Please refer to supplementary multimedia.

Fig. 4 shows the rolling speed (along the lower side of the lumen) for clusters with perimeter in the $50\,\mu m$ to $450\,\mu m$ range. The dashed lines represent the theoretical rolling speed of the clusters, assuming pure rolling motion below the step-out frequency given by Equation (4), indicating that the rolling speed increases with the actuation frequency and the perimeter. The rolling speed is calculated using Equation (5) for clusters with perimeter in the $54\,\mu m$ to $456\,\mu m$ range. The measured rolling speed of the clusters has similar behavior to the theoretical prediction and the rolling speed increases with the actuation frequency and the perimeter, but at a much smaller rate. With the exception of a few clusters in this experiment ($n = 15$), the rolling speed increases with the actuation frequency, implying that their step-out frequency is greater than 10 Hz irrespective of size. At low actuation frequencies (~ 0.1 Hz), large clusters tended to aggregate. As frequency increases, the size of observed clusters decreases. The bonds between aggregated MNPs-coated sperm cells are relatively fragile and interactions associated with increased actuation frequency may cause larger clusters to collapse into smaller ones. By actuating clusters at high frequencies or against the wall of the lumen, it is possible to induce the collapse of larger clusters into smaller ones in this manner, as shown in Fig. 3 at $t = 5$ s. In contrast, actuation of the clusters at relatively low frequencies prevents collapsing into smaller clusters, as shown in Fig. 4(B).

C. Dynamic Magnetic Properties of Magnetic Nanoparticles

Actuated MNPs produce a small signal that can potentially be utilized for sensing. Enhanced biosensing relies on the use of magnetization dynamics, which are primarily governed by time-dependent motion of the magnetization due to externally applied magnetic fields. The super paramagnetic quantifier (SPaQ), illustrated in Fig. 5(A), is a custom-made differential susceptometry device (University of Twente, The Netherlands) developed for fingerprinting of MNPs [8]. SPaQ was used to assess the magnetisation response of MNPs to an alternating field of (1.33 mT) and a small offset field (swept between ± 13.3 mT). Total acquisition time was set to 1 s at the excitation frequency of 1 kHz.

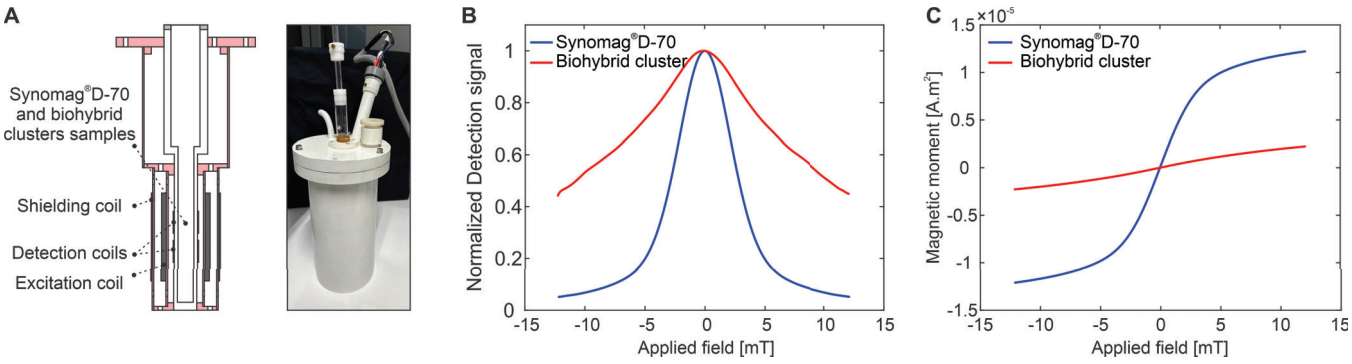

Fig. 5. Constraining the nanoparticles by electrostatic adhesion with the cell membrane yields significant decrease in the magnetometry sensitivity. Schematic of super paramagnetic quantifier (A) used to assess differential magnetic susceptibility (B) and magnetic moment (C) through induction voltage in detection coils as a function of the the applies magnetic field for Synomag®D-70 and for Synomag®D-70-coated sperm cells.

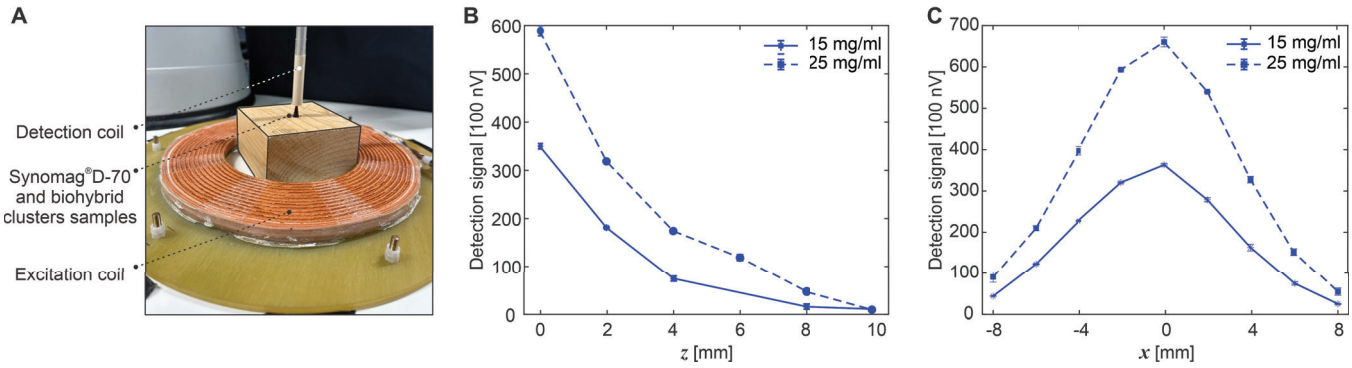

Fig. 6. Experimental differential magnetometer setup showing the excitation coil, detection coils configuration, and the Synomag®D-70 sample (A). The induced voltage in the detecting coils is used to evaluate the system sensitivity regarding the longitudinal (B) and lateral (C) distance between probe and sample. The resolution of the differential magnetometer is less than that of the super paramagnetic quantifier, leading to a negligible signal from the nanoparticles-coated sperm cells.

The dynamic properties of free MNPs and MNPs-coated sperm cells are assessed using 100 µL sample of Synomag®D-70 (concentration 2.5 mg/mL) and biohybrid clusters (concentration 2.5 mg/mL). Fig. 5 shows the magnetic momentum and relative induced voltage in detection coils for both samples. Similarly to previous observations, that the detected signal will decrease with increased size of the MNPs [6], biohybrid clusters consisting of Synomag®D-70-coated sperm cells are reaching their saturation at a larger excitation field than the smaller Synomag®D-70 particles.

D. Localization by Differential Magnetometer

A nonlinear magnetic detection principle, referred to as DiffMag, utilizes nonlinear MNPs characteristics by augmenting an alternating excitation field with a DC offset. Consequently, signal received solely depends on the characteristics of MNPs. In this experiment, a nonlinear magnetic sensing device based upon DiffMag principle, is used for localization. This device has been developed for laparoscopic procedures and employs a separated excitation and detection approach as shown in Fig. 6(A). Signal detection utilizes the differential magnetometry principle to acquire the nonlinear signal originating from the MNPs.

The signal for two 50 µL samples containing pure Synomag®D-70 (i.e. 15 mg/mL, and 25 mg/mL), and one sample containing 100 µL biohybrid sperm clusters coated with Synomag®D-70. All data were acquired threefold for all samples. The detection depth and spatial sensitivity were manipulated using a robotic arm (Meca500, Mecademic inc., Canada) ranging 0-8 mm with 2 mm steps. The signal is measured 20 times per acquisition (10 s). Fig. 6(A-B) illustrates the detection of pure Synomag®D-70 samples. The signal is consistently larger for a sample with higher MNPs concentration and decreases with distance from the sample (laterally and longitudinally). The signal amplitude for a sample with the concentration of 25 mg/mL was consistently 48% (STD = 4) larger. However, the signal originating from biohybrid sperm clusters containing 2.5 mg/mL did not rise above the background noise level.

IV. DISCUSSION

We present an experimental study for magnetic localization of biohybrid microrobots with differential magnetometry. Synomag®D-70 dextran coated iron oxide nanoparticles are utilized, which show excellent magnetization profile and are optimized for magnetic particle imaging. The bare nanoparticles show excellent signal in the magnetometry. The inductive response of the clusters is reduced due to the immobilization of the nanoparticles. The nanoparticles be-

come immobilized when attached to the cell membrane. This inhibits their free oscillation and thus only little detectable response is measured with the laparoscopic differential magnetometer. Further, the signal is dependent on the size of the nanoparticles and their ability to oscillate. Electrostatic attractive forces between the nanoparticles and the membrane restrict this effect and thus reduces the detected signal.

After interacting with the biological membrane, the MNPs experience a reduction in the number of mechanical degrees of freedom for rotation and translation. This influences their magnetic behaviour. Generally, the signal of MNPs is attributed to two processes: Brownian relaxation and Neel relaxation. Brownian relaxation is the physical rotation of the particle, which is dependent on the surrounding viscosity, nanoparticle's hydrodynamic volume and temperature. The Neel relaxation is the internal rotation of magnetization of the core inside the nanoparticles. This characteristic is material dependent. A third relaxation process has recently been discovered in nanoflower-shaped particles like Synomag, attributed to the relaxation of disordered spins within the nanoflower particle [6]. For Synomag MNPs, it is known that its relaxation processes are mostly contributed by internal magnetization processes rather than Brownian relaxation. A decrease in magnetic signal is observed after immobilization of Synomag MNPs to macrophages, but their insensitivity to viscosity changes still renders them most promising for future clinical applications in comparison to other MNPs.

V. CONCLUSIONS

When standard MNPs (used in standard magnetometry) are constrained by the electrostatic adhesive forces with an organic body, they exhibit a negligible oscillating magnetization upon excitation using an alternating field. The rate of change of the magnetization of these MNPs is measured in terms of the induction voltage in a nearby detection coil using two nonlinear differential magnetometry techniques. Using a laparascopic differential magnetometer, the constrained nanoparticles show negligible time-derivative of the oscillating magnetization compared to free MNPs of the same volume. In contrast, the higher sensitivity of the super paramagnetic quantifier shows that the time-derivative of the oscillating magnetization of the constrained MNPs is smaller than that of the free MNPs with one order of magnitude. The results suggest that the fabrication of biohybrid clusters requires further refinement to improve inductive response and actuation simultaneously.

Future research in this field will include functionalization of the MNPs to allow free oscillation, while still being rigidly connected to the sperm cells. One approach is to embed MNPs into a polymer matrix of microparticles with sufficiently large pores. This assembly may be necessary to allow MNPs to move freely within the polymer matrix of microparticles. These polymeric microparticles can then be attached to the biotemplates in a targeted manner, so that imaging of biohybrid microrobots with differential magnetometry can be achieved.

REFERENCES

[1] H. Xu, M. Medina-Sanchez, V. Magdanz, L. Schwarz, F. Hebenstreit, and O. G. Schmidt, "Sperm-Hybrid micromotor for targeted drug delivery."*ACS Nano*, vol. 12, issue 1, pp. 327-337, 2018.

[2] C. K. Schmidt, M. Medina-Sánchez, R. J. Edmondson, and O. G. Schmidt, "Engineering microrobots for targeted cancer therapies from a medical perspective," *Nature Communications*, vol. 11, no. 5618, pp. 1–18, 2020.

[3] Y. Alapan, O. Yasa, B. Yigit, I. C. Yasa, P. Erkoc, and M. Sitti, "Microrobotics and microorganisms: biohybrid autonomous cellular robots," *Annual Review of Control, Robotics, and Autonomous Systems*, vol. 2, pp. 205–30, 2019.

[4] B. Behkam and M. Sitti, "Bacterial flagella-based propulsion and on/off motion control of microscale objects," *Applied Physics Letters*, vol. 90, 023902, 2007.

[5] W. Gao, X. Feng, A. Pei, C. R. Kane, R. Tam, C. Hennessy, and J. Wang, "Bioinspired helical microswimmers based on vascular plants," *Nano Letters*, vol. 14, no. 1, pp. 305–310, 2014.

[6] K. Riahi, M. M. van de Loosdrecht, L. Alic, and B. Haken, "Assessment of differential magnetic susceptibility in nanoparticles: Effects of changes in viscosity and immobilisation," *Journal of Magnetism and Magnetic Materials*, Vol. 514, no. 15, 2020.

[7] Q. Wang, L. Yang, J. Yu, P. W. Y. Chiu, Y.-P. Zheng, and L. Zhang, "Real-Time magnetic navigation of a rotating colloidal microswarm under ultrasound guidance," *IEEE Transactions on Biomedical Engineering*, vol. 67, no. 12, pp. 3403-3412, 2020.

[8] M. M. van de Loosdrecht, S. Draack, S. Waanders, J. G. L. Schlief, H. J. G. Krooshoop, T. Viereck, F. Ludwig, and B. ten Haken, "A novel characterization technique for superparamagnetic iron oxide nanoparticles: The superparamagnetic quantifier, compared with magnetic particle spectroscopy." Rev. Sci. Instrum. 90, 24101 (2019).

[9] M. M. van de Loosdrecht,S. Waanders, H.J.G. Krooshoop, and B. ten Haken, "Separation of excitation and detection coils for in vivo detection of superparamagnetic iron oxide nanoparticles." *Journal of Magnetism and Magnetic Materials* 475, 563–569 (2019).

[10] K. Kamata, Z. Piao, S. Suzuki, T. Fujimori, W. Tajiri, K. Nagai, T. Iyoda, A. Yamada, T. Hayakawa, M. Ishiwara, S. Horaguchi, A. Belay, T. Tanaka, K. Takano, and M. Hangyo, "Spirulina-templated metal microcoils with controlled helical structures for THz electromagnetic responses," *Scientific Reports*, vol. 4, 4919, 2015.

[11] V. Magdanz, J. Gebauer, D. Mahdi, J. Simmchen, and I. S. M. Khalil, "Sperm-templated magnetic microrobots," in *Proceedings of the 2019 International Conference on Manipulation, Automation and Robotics at Small Scales (MARSS),* 2019, pp. 1–6.

[12] X. Yan, Q. Zhou, M. Vincent, Y. Deng, J. Yu, J. Xu, T. Xu, T. Tang, L. Bian, Y.-X. J. Wang, K. Kostarelos, and L. Zhang, "Multifunctional biohybrid magnetite microrobots for imaging-guided therapy," *Science Robotics*, vol. 2, eaaq1155, 2017.

[13] J.-B. Mathieu, G. Beaudoin, and S. Martel, "Method of propulsion of a ferromagnetic core in the cardiovascular system through magnetic gradients generated by an mri system," *IEEE Trans. Biomed. Eng.*, vol. 53, no. 2, pp. 292–299, 2006.

[14] K. I. A. Middelhoek, V. Magdanz, L. Abelmann, and I. S. M. Khalil, "Drug-Loaded IRONSperm clusters: modeling, wireless actuation, and ultrasound imaging," *Biomedical Materials*, vol. 17, no. 6, 65001, 2022.

[15] S. Pane, G. Faoro, E. Sinibaldi, V. Iacovacci, and A. Menciassi, "Ultrasound acoustic phase analysis enables robotic visual-servoing of magnetic microrobots," *IEEE Transactions on Robotics*, vol. 38, no. 3, pp. 1571-1582, 2022.

[16] M. Visscher, S. Waanders, H. Krooshoop, and B. ten Haken, "Selective detection of magnetic nanoparticles in biomedical applications using differential magnetometry," *Journal of Magnetism and Magnetic Materials*, vol. 365, pp. 31–39, 2014.

[17] J. M. S. Dias, D. Estima, H. Punte, A. Klingner, L. Marques, V. Magdanz, and I. S. M. Khalil, "Modeling and characterization of the passive bending stiffness of nanoparticle-coated sperm cells using magnetic excitation," *Advanced Theory and Simulations*, vol. 5, no. 3, 2100438, 2022.

[18] S. Waanders, M. Visscher, R. R. Wildeboer, T. O. B. Oderkerk, H. J. G. Krooshoop, and B. ten Haken, "A handheld-based sentinel lymph node mapping device using differential magnetometry," *Physics in Medicine & Biology*, vol. 61, pp. 8120–8134, 2016.